Applied Catalysis B: Environmental 134–135 (2013) 367–380

Contents lists available at SciVerse ScienceDirect

Applied Catalysis B: Environmental

journal homepage: www.elsevier.com/locate/apcatb

Selective catalytic reduction of NO with NH_3 over Cr-ZSM-5 catalysts: General characterization and catalysts screening

F. Ayari[a,*], M. Mhamdi[a], J. Álvarez-Rodríguez[b], A.R. Guerrero Ruiz[b], G. Delahay[c], A. Ghorbel[a]

[a] Laboratoire de Chimie des Matériaux et Catalyse, Département de Chimie, Faculté des Sciences de Tunis, Campus Universitaire Tunis ElManar, 2092 Tunis, Tunisia
[b] Unidad Asociada Group for Desig. and Appl. of Heter. Catal. UNED-ICP (CSIC), Dpto. Inorganic and Technical Chemistry, Faculty of Sciences, UNED, 28040 Madrid, Spain
[c] Institut Charles Gerhardt Montpellier, UMR 5253, CNRS-UM2-ENSCM-UM1, Eq. "Matériaux Avancés pour la Catalyse et la Santé", ENSCM (MACS - Site la Galéra), 8, rue Ecole Normale, 34296 Montpellier Cedex 5, France

ARTICLE INFO

Article history:
Received 18 September 2012
Received in revised form
10 December 2012
Accepted 7 January 2013
Available online 26 January 2013

Keywords:
Ammonia
Cr-ZSM-5
Selective catalytic reduction (SCR)
Solid-state ion exchange
UV–vis DRS
XPS spectroscopy

ABSTRACT

Cr exchanged ZSM-5 catalysts (Cr/Al = 1) prepared by solid-state ion exchange were tested in SCR of NO with ammonia. Since $CrCl_3$ precursor sublimates during the solid-state reaction, chromate species were stabilized in the exchange sites of H^+-ZSM-5 (Si/Al = 15) and Cr_2O_3 formation is, therefore, limited. However, using Cr nitrate and NH_4^+-ZSM-5 (Si/Al = 26) zeolite, massive particles of α-Cr_2O_3 occupied the catalyst surface. At the contrary, well-dispersed particles of Cr_2O_3 were detected with H^+-ZSM-5 and Cr nitrate precursor. Starting from Cr acetate precursor, agglomerates of amorphous oxide were detected with H^+-ZSM-5 like support. In the temperature range 50–300 °C, Cr chloride and Cr nitrate precursors and H^+-ZSM-5 led to highly active catalysts, while Cr nitrate and NH_4^+-ZSM-5 led to a poorly active catalyst. However, catalysts issued from Cr acetate are promising in SCR but inefficient agglomerates of oxide (amorphous or crystalline chromia) could be avoided with NH_4^+-ZSM-5 like support.

1. Introduction

Nowadays, air quality is taken as a major aspect of the quality of life leading to sustainable development in many areas of the world. However, countries that are rapidly developing and urbanizing will experience the most health problems due to air pollution.

Tunisia country is situated on the Mediterranean coast of North Africa with almost 165,000 square kilometers in area and an estimated population of 10.6 million [1]. In Tunisia, a large contribution to the air pollution provides from nitrogen oxides (NO_x) associated with transportation and inefficient techniques used in industry. However, to improve the government's performance in putting sustainability at the heart of its policies and programs, a range of options, including the creation of the ANPE (Agence Nationale de Protection de l'Environnement), was examined. Since their foundation in 1988, the ANPE operated only 17 stations in different Tunisian localities in order to control the emissions of hazardous compounds originating from diesel engines, especially soot and NO_x. Table 1 represents the evolution of NO_x emissions which mainly provided from agricultural and industrial activities in Tunisia [1].

The data illustrated in Table 1 evidencing that NO_x emissions have been increasing steadily and may reach potential levels in the next years if current development patterns persist. Therefore, the government of Tunisia should develop aggressive strategies to address climate change and air quality by taking action to reduce greenhouse gases and air pollution.

Selective catalytic reduction (SCR) is considered to be the most efficient technology for reducing NO_x emissions from stationary sources. Efficient reaction (Eq. (1)) can be achieved by conventional catalysts such as V_2O_5-WO_3/TiO_2 [2].

$$2NO + 2NH_3 + \frac{1}{2}O_2 \rightarrow 2N_2 + 3H_2O \quad (1)$$

The most effective reaction temperature for this process is known to be in the range of 300–400 °C [3,4]. However, researchers in the field of academia and industry continue to develop new low-temperature SCR catalysts that can work well around 250 °C or even below, in which the SCR unit could be placed behind the electric precipitation and desulfurizer in power plant and efficiently remove NO_x at wider temperature range for NO_x control in diesel engine [5]. According to literatures, many catalysts, e.g., modified carbon fibers [6] and metal-activated carbon [7], have been tested in SCR of NO at low temperatures (<250 °C). However, such

* Corresponding author. Tel.: +216 50646504; fax: +216 71885008.
E-mail address: lcmc_fa@yahoo.fr (F. Ayari).

0926-3373/$ – see front matter.
http://dx.doi.org/10.1016/j.apcatb.2013.01.026

Table 1
NO_x emissions in Tunisia country.

	1995	2005
Agricultural NO_x emission (% of total)	60	66
Industrial NO_x emission (% of total)	9	4
NO_x emission (Thousand metric ton of CO_2 equivalent)[a]	2068	2366

[a] 1 metric ton of CO_2 is released to the atmosphere for every 103 gallons of gasoline used, using a car that gets 25 miles to the gallon.

catalysts exhibited lower catalytic activity for a commercial process. On the other hand, catalysts containing transitional metal such as Mn [8], V [9] and Fe [10] exhibited good low-temperature SCR activity. Among them, the nano-MnO_x catalyst has been studied extensively since it contains various types of labile oxygen species required for low-temperature SCR [5,11].

Several studies have shown that chromium based catalysts, e.g., amorphous and crystalline chromia [12], chromia supported on TiO_2 (anatase) [13,14], chromium spinels: MCr_2O_4 (M = Mg, Zn, Co, Ni, Fe and Cu) [15] and sol–gel derived Cr/Al_2O_3 catalysts [16] can display higher activity in SCR of NO with NH_3 in the presence of excess oxygen. Extensive studies [13,14,17–19] performed with Cr_2O_3/TiO_2 catalysts (0–30 wt.% Cr) have been carried out on samples calcined at low temperature (300 °C) as the investigators wished to stabilize amorphous chromia on the titania surface rather than the undesired crystalline α-Cr_2O_3. Accordingly, Fountzoula et al. [14] reported that higher SCR activity over Cr_2O_3/TiO_2 catalysts provided from isolated Cr(VI) surface species. On the other hand, Schneider et al. [17] pointed out that, upon chromia catalysts, Brönsted-bounded ammonia is crucial for SCR reaction while the direct oxidation of Lewis-bounded ammonia produced mostly N_2O. In our previous study [16], we reported that aerogel Cr/Al_2O_3 solids exhibited higher catalytic activity in SCR of NO than xerogels. In fact, the nature of active sites is governed by the preparation method and the alcogel drying mode. Generally, mono and polychromate species are required for SCR of NO, while Cr^{3+} ions incorporated inside the alumina matrix should be avoided.

Among the new emerging SCR catalytic systems for mobile applications, many efforts are focused on metal promoted zeolites, which had been already proposed in the past for NO_x abatement in stationary installations as well. Many ion exchanged zeolites were reported to be active in SCR of NO with NH_3, such as Fe [20], Mn [21], Cu [22] Ce [23] and Cu [24], and their catalytic activities at low and high temperatures exceeded those of commercial vanadia-based catalysts [25]. For example, Choi et al. [24] reported that Cu ions exchanged with mordenite offered additional adsorption sites for NO and NH_3, which benefited NO reduction mainly at low temperatures. However, Cu ions exchanged with faujasite-type zeolite [26] exhibited catalytic activity at very low temperatures (< 50 °C) which attained a maximum at about 120 °C (70% of selectivity toward N_2).

Several methods, including impregnation, conventional aqueous ion exchange, improved aqueous ion exchange, solid-state ion exchange and chemical vapor ion exchange [27–30] were reported to prepare zeolite catalysts for SCR of NO with NH_3. Delahay et al. [27] investigated SCR of NO over Fe/ZSM-5 catalysts issued from either the sublimation method (Fe salts are acetylacetonate and chloride) or aqueous exchange using Fe nitrate. The authors [27] reported higher deNO_x activity for the catalyst issued from $FeCl_3$, while the mechanical mixture α-Fe_2O_3/ZSM-5 does not exhibit any significant activity. The main difference in catalytic activities has been ascribed to the different contents of active species over Fe/zeolite catalysts under different experimental conditions.

In view of the above it seems to us quite interesting, at least from the scientific viewpoint, to investigate the physicochemical and catalytic properties of Cr-ZSM-5 catalysts. In fact, there is a lack of literature data concerning such a catalyst system. However, Salker et al. [31] investigated SCR of NO with NH_3 over a unique Cr-ZSM-5 catalyst (3.25 wt.% Cr) prepared by wet impregnation method using H^+-ZSM-5 (Si/Al = 20) and Cr nitrate solution. The catalytic test was performed with 1200 ppm NO, 1200 ppm NH_3 in N_2 and 6.5% of O_2 by volume, a space velocity of 180,000 h^{-1} and 0.2 g of catalyst. The authors [31] reported that the presence of H_2O has poisoning effect toward N_2 selectivity.

The aim of this work is studying SCR of NO with NH_3 over Cr-ZSM-5 catalysts prepared by solid-state exchange of different Cr precursors (acetate, chloride and nitrate) with ZSM-5 zeolites (Si/Al = 15 and 26). Different characterization techniques have been adopted in order to study the physicochemical properties of the prepared solids. The chemical composition of different solids has been determined by inductively coupled plasma (ICP). The solid-state exchange of Cr salts with zeolites has been studied by thermal analysis coupled with mass spectrometry (TA/MS). Textural, structural and morphological studies have been performed by physisorption of N_2 at −196 °C, X-ray diffraction (XRD) and transmission electron microscopy (TEM), respectively. Information about the metal oxidation states was obtained by UV–vis diffuse reflectance spectroscopy (DRS), Raman and X-ray photoelectron spectroscopy (XPS). The redox features were investigated by temperature-programmed method using a hydrogen flow (H_2-TPR), while the catalysts acidity was studied by temperature-programmed desorption of ammonia (NH_3-TPD) and diffuse reflectance infrared Fourier transform spectroscopy (DRIFTS).

2. Experimental

2.1. Catalysts preparation

The catalysts were prepared by solid-state ion exchange by mixing 1 g of H^+-ZSM-5 zeolite (Si/Al = 15), furnished by Zeolyst, in a mortar and pestle with the desired Cr loading (Cr/Al = 1: 0.16 g of Cr chloride (Prolabo), 0.41 g of Cr nitrate (Acros Organics, 99%) and 0.21 g of Cr acetate (Strem Chemicals)). The finely ground powders were heated for 12 h at 500 °C in helium flow (30 cm^3/min, 2 °C/min). Additional catalysts were prepared using the same procedure than above with NH_4^+-ZSM-5 (Si/Al = 26) as starting zeolite and using Cr nitrate and Cr acetate like precursors (Cr/Al = 1: 0.24 g of Cr nitrate and 0.14 g of Cr acetate). Catalysts were labeled and stored as Chl-15, Nit-15, Nit-26, Ac-15 and Ac-26.

2.2. Catalysts characterization

The elemental content of Cr, Si and Al was determined by chemical analysis of the catalysts at the Vernaison Center of the CNRS (France) employing ICP. TA/MS analysis was performed using a SDT Q600 apparatus with ∼30 mg of precursor/zeolite mixture (Cr/Al = 1). A thermal treatment in helium (30 cm^3/min, 5 °C/min) between 30 and 700 °C (30–900 °C in the case of $CrCl_3$) was applied. The chemical composition of gaseous products was determined using a mass spectrometer piloted with Quadstar 32 Bits software. N_2 adsorption–desorption isotherms were determined with an automatic ASAP 2000 apparatus from Micromeritics. Specific surface area was determined by BET method, microporous volume by *t*-plot method and porous volume is the volume adsorbed at P/P°=0.98. XRD measurements were performed on an X'Pert Pro X-ray diffractometer from PANalytical with Cu Kα radiation (λ=1.54060 Å), generator setting of 40 kV and 40 mA, a scanning speed of 0.05°/min, and a scanning region of 2–70°. The diffractometer was operated at 1.0° diverging and 0.1° receiving slits and a continuous intensity trace was recorded as function of 2θ. Structural data identification was performed using EVA software. Information about the metal particles in the catalysts was obtained

Table 2
Chemical analysis results.

Sample	Cr wt.%	Al wt.%	Si/Al mol/mol	Cr/Al mol/mol	Ion exchange degree (%)[a]
H^+-ZSM-5	–	2.60	15.12	–	–
NH_4^+-ZSM-5	–	1.40	27.38	–	–
Ac-15	5.13	2.19	15.12	1.20	363
Chl-15	1.39	2.19	15.03	0.33	100
Nit-15	4.46	2.24	15.36	1.06	318
Ac-26	3.06	1.30	27.02	1.22	366
Nit-26	2.16	1.33	27.53	0.84	252

[a] Defined by 300 × Cr/Al (mol/mol) if we consider that Cr^{3+} ions are only the possible exchange species.

by TEM. The measurements were performed in a JEOL JEM-2000 FX Electron Microscope (200 kV) provided with an X-ray energy dispersive spectroscopy system (XEDS). The catalyst samples were suspended and dispersed by ultrasonic treatment in acetone. A drop of the fine suspension was placed on a copper TEM grid, which was then loaded into the microscope. UV–vis DRS analysis was performed on a Perkin Elmer Lambda 45 spectrophotometer equipped with a diffuse reflectance attachment. Spectra were recorded at room temperature in the wavelength range 900–200 nm using the parent zeolites as reference materials. Raman measurements were carried out on a confocal Thermo Scientific DXR Raman Microscopy system using the visible line at 532 nm and an incident power of 10 mW. XPS spectra were recorded on a SSX 100/206 photoelectron spectrometer equipped with a monochromatized micro focused Al X-ray source (1486.6 eV, powered at 20 mA and 10 kV). H_2-TPR profiles were obtained on a Micromeritics Autochem 2910 analyzer, in a Pyrex U-tube reactor and an on-line thermal conductivity detector (TCD). The catalyst (70 mg) was dried in air at 500 °C for 1 h and reduced from 50 to 1000 °C (15 °C/min) with H_2 (3%)/Ar flow. NH_3-TPD analysis was performed with the same H_2-TPR analyzer. As the automatic NH_3-TPD program included a pretreatment in air, the sample (40 mg) was first exposed to an air flow (10 cm^3/min) at 500 °C for 1 h, then saturated with flowing ammonia at 100 °C and flushed with helium at the same temperature. Finally, the temperature was ramped to 700 °C (10 °C/min). The outlet H_2O was trapped at low temperature (–40 °C) in a mixture of liquid N_2/propan-2-ol before reaching the TCD. DRIFT spectra were recorded on a Bruker IFS 55 spectrometer equipped with a Thermo Spectra Tech reacting cell at a spectral resolution of 4 cm^{-1} and accumulating 200 scans. Samples were activated in situ at 500 °C in helium (30 cm^3/min, 5 °C/min).

The catalytic tests were performed in a flow reactor operating at atmospheric pressure. Catalyst aliquots (20 mg, or 0.025 cm^3) were activated in situ at 450 °C in air and cooled to room temperature. The catalytic tests were carried out in temperature programmed surface reaction (TPSR) from 50 to 450 °C at 7.5 °C/min with a space velocity of 332,000 h^{-1} using the following gas composition: 0.2% NO, 0.2% NH_3, 3% O_2 and 96.6% He. The effluent composition was monitored continuously and by sampling on line to a quadruple mass spectrometer (Balzers QMS 200) equipped with Channeltron and Faraday detectors (0–200 amu).

Catalytic results were expressed as follows:

$$\text{Conversion of reactant } (i): X_i = \frac{(R_i)_0 - (R_i)_T}{(R_i)_0} \times 100$$

$(R_i)_0$ and $(R_i)_T$: are respectively the reactant (i) concentrations at the inlet gas reactor and at the T temperature.

Selectivity to N_2O is expressed as: $S_{N_2O} = \left[\frac{2F_{N_2O}}{F_{NO_{in}} + F_{NH_{3in}} - F_{NOout} - F_{NH_{3out}}}\right] \times 100$ where F_{N_2O} is the molar flow rate (mol/s) of N_2O, and in and out refer to the reactor inlet and outlet, respectively. N_2O quantification was performed using a known amount of N_2O 1% in helium.

Selectivity to N_2 is expressed as: $S_{N_2} = 100 - S_{N_2O}$

3. Results and discussion

3.1. Chemical analysis

Table 2 gives the elemental analysis of parent zeolites and the prepared solids including Cr, Al contents, Si/Al and Cr/Al molar ratios. Besides elemental analysis, Table 2 summarized the resulting ion exchange degrees. As expected, Si/Al ratio values fit the data provided by the zeolite manufacturer. On the other hand, the Cr contents analyzed in the final catalysts depended on the precursor nature. Using Cr nitrate and Cr acetate precursors, the metal content in the final catalysts is consistent with what was expected. However, another process probably occurs with $CrCl_3$ since the Cr content is much lower. Concerning the ion exchange degrees, the data illustrated in Table 2 evidenced that Ac-15, Ac-26, Nit-15 and Nit-26 solids are over-exchanged, while Chl-15 solid contains enough Cr ions required for 100% of exchange.

ZSM-5 zeolite exhibits a three-dimensional intersecting channel system (a straight channel of 0.56×0.53 nm and a sinusoidal channel of 0.55×0.51 nm) [32]. Thus, higher Si/Al molar ratios, i.e., Si/Al = 15 and 26, and medium pores do not allow the totality of Cr^{3+} ions to occupy positions where it is possible to balance the charges of three $(Si–O–Al)^-$ groups. As bare Cr cations cannot exist, it is possible to have the presence of (hydr)oxo-cation species like $[OH—Cr—O—Cr—OH]^{2+}$, similarly to Fe/ZSM-5 system [27], and/or Cr oxide species.

3.2. TA/MS study

The different weight losses observed during the thermal treatment of different precursors and mixtures are compiled in Table 3. Our thermal analyses focus also on the interaction developed between the different Cr precursors and the zeolites. A proposed measure of the interaction strength is α-parameter [33] defined as:

$$\alpha = \frac{\%WL_s \times 100}{\%WL_{us}}$$

where WL_{us} is the total weight loss observed upon unsupported Cr precursors while WL_s is the total weight loss observed upon Cr precursors supported on zeolites.

In the Table 3 it is seen that, for the same type of support, α-values increase from Chl-15 over Ac-15 to Nit-15. This result indicates the low affinity of $CrCl_3$ precursor toward H^+-ZSM-5 (Si/Al = 15). However, when compared to Cr acetate, Cr nitrate precursor exhibits a better affinity toward H^+-ZSM-5 due to its lower thermal stability [34]. For the same type of Cr precursor, α-values decrease with increasing Si/Al molar ratio since the amount of sites available for Cr exchange depends on Al content.

Fig. 1a illustrates TG curve of $CrCl_3$ treated in helium while Fig. 1b and c represents, respectively, the evolution of gaseous products during the thermal treatment of $CrCl_3$ and $CrCl_3$/H^+-ZSM-5 mixture in helium. The detected MS fragments are those of H_2O^+

Table 3
Thermal analysis results: weight losses and α-values.

	Different weight losses (%) and the corresponding temperature range (°C)	α (%)[a]
Cr acetate (He)	7.23 (30–170), 53.61 (250–500), 4.00 (500–700)	––
Cr acetate (O_2)	12.74 (30–200), 44.21 (200–400), 9.52 (400–700)	
Cr acetate/H^+-ZSM-5[b] (He)	4.78 (30–250), 8.90 (250–500)	22.48
Cr acetate/NH_4^+-ZSM-5[c] (He)	2.79 (30–180), 0.44 (180–240), 6.92 (250–500)	16.68
Cr nitrate (He)	4.77 (30–63), 22.89 (63–100), 44.70 (100–250), 6.15 (250–500)	–
Cr nitrate/H^+-ZSM-5[b] (He)	9.44 (30–116), 11.71 (116–210), 1.10 (310–473)	28.70
Cr nitrate/NH_4^+-ZSM-5[c] (He)	6.17 (30–111), 8.58 (111–212), 0.49 (400–480)	19.66
Cr chloride (He)	0.65 (30–80), 0.97 (80–140), 92.32 (140–900)	–
Cr chloride/H^+-ZSM-5[b] (He)	2.05 (30–100), 1.49 (100–230), 8.10 (230–650)	12.61

[a] $\alpha = \%WL_s \times 100/\%WL_{us}$.
[b] H^+-ZSM-5 (Si/Al = 15).
[c] NH_4^+-ZSM-5 (Si/Al = 26).

(m/z = 18), Cl^+ in HCl (m/z = 35, 36, 37 and 38) and Cl_2^+ (m/z = 70, 72 and 74).

Fig. 1(a and b) and Table 3 show that $CrCl_3$ exhibited a weight loss of 1.62% (30–140 °C, endothermic peaks at 60 and 120 °C) which corresponds to the salt dehydration. However, the significant weight loss of 92.32% observed at higher temperatures as well as MS results (evolution of Cl_2^+ fragment in Fig. 1b) belong to $CrCl_3$ sublimation [35] according to the following equilibriums [36]:

$$CrCl_{3(sd)} \leftrightarrow CrCl_{3(g)}$$

$$2CrCl_{3(sd)} \leftrightarrow CrCl_{2(sd)} + CrCl_{4(g)}$$

$$CrCl_{2(sd)} \leftrightarrow CrCl_{2(g)}$$

$$CrCl_{4(g)} \leftrightarrow CrCl_{2(g)} + Cl_{2(g)}$$

In the presence of zeolite, the thermal analysis results (Table 3) revealed two weight losses of 3.54% (30–230 °C) and 8.1% (230–650 °C). On the other hand, Fig. 1c showed the evolution of H_2O and HCl during the thermal treatment of $CrCl_3$/H^+-ZSM-5 mixture. The first weight loss would correspond to the mixture dehydration while the second one corresponds to the exchange of H^+-ZSM-5 with $CrCl_3$ according to Eq. (2):

$$CrCl_3 + 3H\text{-O-zeolite} \rightarrow 3HCl + Cr^{3+}(\text{-O-zeolite})_3 \quad (2)$$

The lower amount of Cr over Chl-15 solid (1.39 wt.% Cr, Table 2) and the lower value of α-parameter (12.61%, Table 3) belong to the sublimation of $CrCl_3$ in the mixture even gaseous chlorine has not been detected by MS (Fig. 1c). Sole et al. [37] reported that the rate of $CrCl_3$ vaporization in a nitrogen stream depended on the salt granulometry. In fact, pelletizing a $CrCl_3$ sample, i.e., minimizing its surface area, inhibits the vaporization of the salt. In our study, an intimate mixture of $CrCl_3$ and H^+-ZSM-5 would inhibit the sublimation.

TA/MS study performed with unsupported Cr nitrate precursor as well as Cr nitrate/zeolite mixtures revealed the presence of different MS fragments: NH_3^+ (m/z = 17), H_2O^+ (m/z = 18), N_2^+ (m/z = 29), NO^+ (m/z = 30), O_2^+ (m/z = 32), N_2O^+ (m/z = 44), NO_2^+ (m/z = 46) and HNO_3^+ (m/z = 63). On the other hand, the thermal decomposition schemes of the different mixtures (results not shown) contain the same features that of pure Cr nitrate. From TA/MS results, it can be deduced that Cr nitrate precursor decomposes into Cr_2O_3 according to the mechanism previously described [34,38]. Moreover, such a mechanism is also suitable for Cr nitrate/zeolite mixtures (see weight losses in Table 3).

Let us assume that area under $I_{m/z}(T)$ curve (where $I_{m/z}(T)$ is ionic current corresponding to the ion which indicated m/z value) is related to the total amount of gas product identified by m/z value (for example m/z = 18 corresponds to H_2O^+). Now it is possible to determine the degree of decomposition $\alpha_{m/z=18}$ (T) as a function of temperature T, in respect to H_2O, a product of decomposition, according to the following definition:

$$\alpha_{m/z=18}(T) = \frac{\int_0^T TI_{m/z=18}(T)\,dT}{\int_0^{T_k} TI_{m/z=18}(T)\,dT}$$

where T_k is temperature at which H_2O (m/z = 18) stops to evolve [34].

Fig. 2a represents the evolution of H_2O^+ fragment during the thermal decomposition of Cr nitrate/zeolite mixtures, while Fig. 2b represents the evolution of $\alpha_{m/z=18}$ as a function of temperature.

According to Fig. 2 (a and b), the dehydration of both precursor and zeolite is more pronounced over Cr nitrate/H^+-ZSM-5 mixture. At the contrary, Cr nitrate/NH_4^+-ZSM-5 mixture exhibited a slow dehydration throughout the temperature range 30–150 °C.

During the thermal treatment of Cr acetate/zeolite mixtures and unsupported Cr acetate precursor, the detected MS fragments are those of CH_4^+ (m/z = 16), H_2O^+ (m/z = 18), CO^+ (m/z = 28), CH_2O^+ (m/z = 30), CH_3CO^+ (m/z = 43), CO_2^+ (m/z = 44), $COOH^+$ (m/z = 45) and CH_3COOH^+ (m/z = 60) [39]. The evolution of various MS fragments

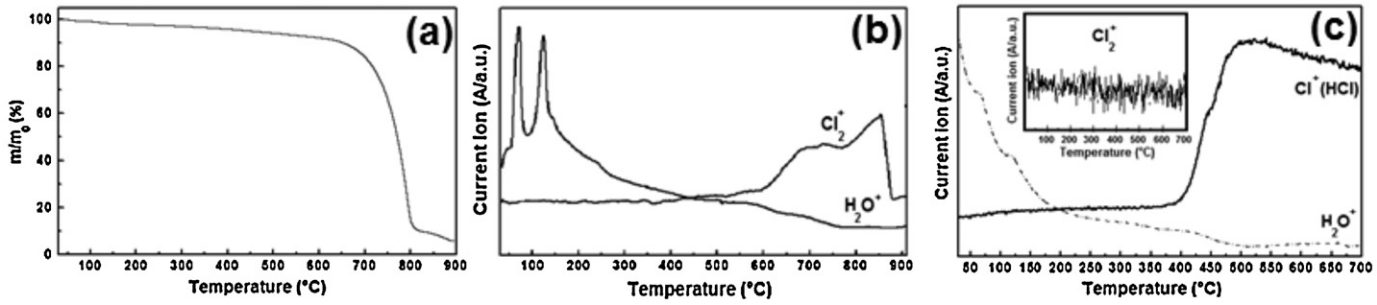

Fig. 1. (a) TG curve of $CrCl_3$, (b) Evolution of gaseous products during the thermal decomposition of $CrCl_3$ in helium, (c) Evolution of gaseous products during the thermal decomposition of $CrCl_3$/H^+-ZSM-5 mixture in helium.

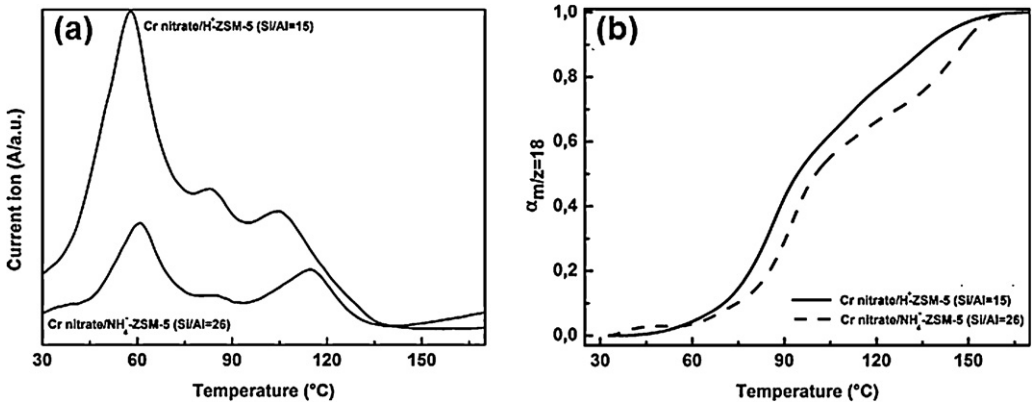

Fig. 2. (a) Evolution of H_2O^+ fragment during the thermal decomposition of Cr nitrate/zeolite mixtures, (b) Degree of decomposition of Cr nitrate/zeolite mixtures in respect to H_2O.

Table 4
Textural properties of the investigated solids.

Sample	S_{BET} (m^2/g)	Microporous surface (m^2/g)	Microporous volume (cm^3/g)	Mesoporous volume (cm^3/g)	Porous volume (cm^3/g)	r_s, r_v
H^+-ZSM-5 (15)	340	198	0.12	0.14	0.26	0.71, 1.16
NH_4^+-ZSM-5 (26)	312	239	0.14	0.10	0.24	0.30, 0.71
Ac-15	319	185	0.10	0.14	0.24	0.72, 1.40
Chl-15	304	186	0.11	0.12	0.23	0.63, 1.09
Nit-15	248	161	0.10	0.10	0.20	0.54, 1.00
Ac-26	336	197	0.11	0.41	0.52	0.70, 3.72
Nit-26	353	212	0.12	0.40	0.52	0.66, 3.33

and the total weight loss obtained in oxygen stream (Table 3) indicate that Cr_2O_3 is the final product of Cr acetate decomposition in helium. However, the solid-state exchange of Cr acetate with H^+-ZSM-5 takes place in the temperature range 250–500 °C according to the mechanism previously proposed [39].

Mavrodinova [40] reported that the individual electrostatic fields of the different zeolite cations (H^+ and NH_4^+) does not influence the process of solid-state exchange of NH_4Cl into beta zeolites. In our study, NH_4^+-ZSM-5 zeolite is already deammoniated at lower temperatures and the mechanism previously proposed [39] is suitable for both Cr acetate/zeolite mixtures.

3.3. Textural, structural and morphological studies

Ac-15, Chl-15 and Nit-15 solids as well as H^+-ZSM-5 zeolite exhibit a type I isotherm, evidencing a microporous texture. However, Ac-26 and Nit-26 and the corresponding support (NH_4^+-ZSM-5) exhibit a type IV isotherm, indicative of the mesoporous character of such solids. Textural properties are summarized in Table 4.

In the Table 4, it is seen that exchanging Cr ions slightly decreases the specific surface area and the porosity of H^+-ZSM-5 (Si/Al = 15) due to the presence of extra-framework aluminum species and/or Cr oxide aggregates inside the pores and channels. Nevertheless, this effect has not been observed with Ac-26 and Nit-26 solids. In order to explain such a behavior, the external to internal surface ratios, r_s, and the mesoporous to microporous volume ratios, r_v, are proposed as practical parameters to classify the prepared solids with respect to their microstructure [41]. According to Table 4, H^+-ZSM-5 (Si/Al = 15), a pure microporous solid, exhibited r_s and r_v parameters values of 0.71 and 1.16, respectively, while r_s and r_v values obtained with Ac-15, Chl-15 and Nit-15 solids do not differ significantly from those of support, which indicates a similar texture. At the contrary, NH_4^+-ZSM-5 (Si/Al = 26) solid exhibited r_s and r_v parameters values of 0.30 and 0.71, respectively, while higher r_s and r_v parameters values were obtained with Ac-26 and Nit-26 solids (see Table 4), which indicates the presence of some degree of mesoporosity. Gervasini [41] reported a similar behavior with cobalt and nickel loaded ZSM-5 zeolite.

XRD patterns of the different materials are shown in Fig. 3. The prepared catalysts exhibited diffraction peaks which are typical for crystalline ZSM-5 [42], but the presence of Cr oxide aggregates on the outer surface is not excluded since they would not be detected by XRD. However, XRD patterns of Nit-15 and Nit-26 solids (Fig. 3d and g, respectively) reveal clear additional peaks attributable to crystalline Cr_2O_3 [38], issued from the thermal decomposition of Cr nitrate under the oxidizing atmosphere of NO_2. However, the deep examination of Fig. 3d and g reveals that α-Cr_2O_3 diffraction peaks differ in shape. Even if broader peaks were detected in the case of

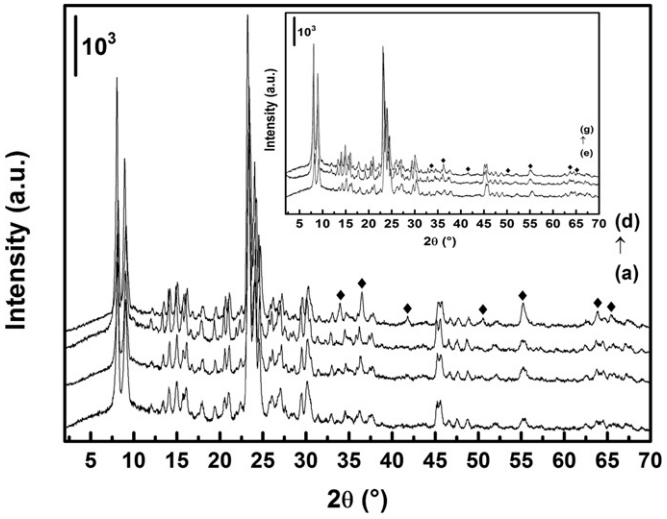

Fig. 3. XRD patterns of (a) H^+-ZSM-5, (b) Ac-15, (c) Chl-15 and (d) Nit-15 solids. Fig. in-set: XRD patterns of (e) NH_4^+-ZSM-5, (f) Ac-26 and (g) Nit-26 solids. (♦): α-Cr_2O_3.

Nit-26 solid, the estimation of the average particle diameters using the Debye–Scherrer method [43] should be avoided since some α-Cr_2O_3 reflections overlap with those of the zeolite lattice.

TEM micrographs of the prepared solids are presented in Fig. 4a–e. Studies of TEM micrographs and XEDS analysis over several regions of Ac-15 sample (Fig. 4a) reveal a chemical composition of Si, Al and Cr, only. Mainly shapes are rhombohedral-like particle (FX2723 and FX2725), which mainly loading silica, and erratic spherical agglomerates of chromia (FX2725) which suggest a low apparent dispersion of Cr_2O_3 particles (less than the nominal). At the contrary, analysis of Ac-26 sample (Fig. 4b) does not reveal highly developed crystalline phase among zeolite aggregates. However, the presence of chemical contents of Si and Al was confirmed by XEDS, while Cr is rather distributed with some spots which load up to 7 wt.%. Analysis of Nit-15 sample by TEM (Fig. 4c) showed up some crystalline phases among zeolite aggregates with apparent square/rhombohedral shapes, where mainly the presence of Si was revealed by XEDS, while Cr is well-dispersed with some spots that load up to 12 wt.%. Nevertheless, TEM micrographs of Nit-26 sample reveal randomly-shaped oxide particles. XEDS analysis in different sample sites confirms the abundance of Si and Al, while Cr is heterogeneously dispersed with distributed spots of higher contents, as FX2945 (43 wt.%). For Chl-15, in a similar proceeding way, without unexpected elements found, half-built polygon-like particles are observed, with stacked chromia particles heterogeneously dispersed (which diffraction pattern reveal quaternary axes) between "apparent spongy" silica (FX3100).

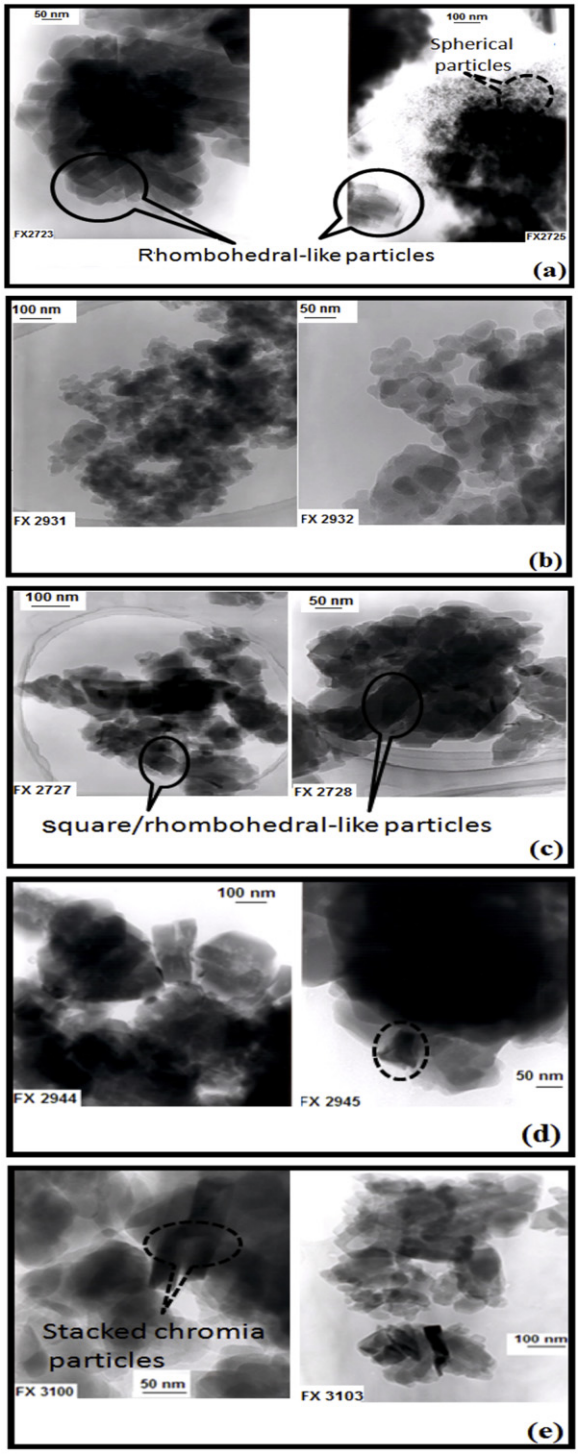

Fig. 4. TEM images of (a) Ac-15, (b) Ac-26, (c) Nit-15, (d) Nit-26 and (e) Chl-15.

In this study, the morphology of oxide species over the prepared solids depended on three crucial parameters: the nature of Cr precursor, Si/Al molar ratio and the deaquation degree. Starting from NH_4^+-ZSM-5 (Si/Al = 26) and Cr nitrate like precursor, agglomerates of α-Cr_2O_3 were rather formed. Li et al. [38] reported that hydrate water displayed a crucial effect during the thermal decomposition of Cr nitrate salt into crystalline Cr_2O_3. In fact, Cr_2O_3 crystal growth depended on the quantity of hydrate water which provides surface hydroxyls that act as binders making aggregates. In our study, MS results (Fig. 2a and 2b) showed that the highest residual water amounts were detected over Cr nitrate/NH_4^+-ZSM-5 (Si/Al = 26) mixture throughout the temperature range 30–150 °C. At the contrary, less residual water amounts were detected over Cr nitrate/H^+-ZSM-5 (Si/Al = 15) mixture and smaller Cr oxide particles were expected.

Starting from Cr chloride and H^+-ZSM-5 zeolite, $CrCl_3$ evaporates during the solid-state exchange process and the formation of Cr_2O_3 occurs to a low extent.

Using Cr acetate like precursor, the morphology of Cr oxide depended on Si/Al molar ratio. It is well-known that ZSM-5 zeolites have a three-dimensional intersecting channel system, a straight channel of 0.56 nm × 0.53 nm runs along the (0 1 0) direction and a sinusoidal channel of 0.55 nm × 0.51 nm runs parallel to the (1 0 0) direction [32]. On the other hand, the ion exchange degree depends on the number of cation exchange sites in ZSM-5 zeolite, which is determined by the framework Si/Al ratio. H^+-ZSM-5 zeolite, due to its lower Si/Al molar ratio (∼15), should present higher cation population and thereby more exchange sites than NH_4^+-ZSM-5 (Si/Al = 26). Nevertheless, according to the data consigned in Table 2, Ac-15 and Ac-26 solids exhibited similar ion exchange degrees. Since Cr cations are polarizable, the main access of these ions is through 10-membered-ring pores of ZSM-5 with an aperture dimension of ∼0.56 nm. However, a highly charged framework of H^+-ZSM-5 would contain narrower 10-ring apertures which reduce the diffusion of Cr ions to the exchange sites. At the contrary, Cr ions may reach the exchange sites of NH_4^+-ZSM-5 and the formation of Cr oxide is therefore limited. In the case of Cr(III) exchanged mordenite [44], Si/Al molar ratio as well as the zeolite pore aperture played a key role in determining the exchange level.

3.4. DRS, Raman and XPS studies

UV–vis DRS spectra of the prepared solids are presented in Fig. 5a and b, while Table 5 illustrated the position of different DRS bands with assignment as well as *B* and μ-parameters values. In the case of d^3 cations, such as Cr^{3+}, Racah parameter (*B*), which reflects the covalency of Cr—O bond in a complex, could be determined experimentally from DRS spectra [45]. In fact, the energy value of

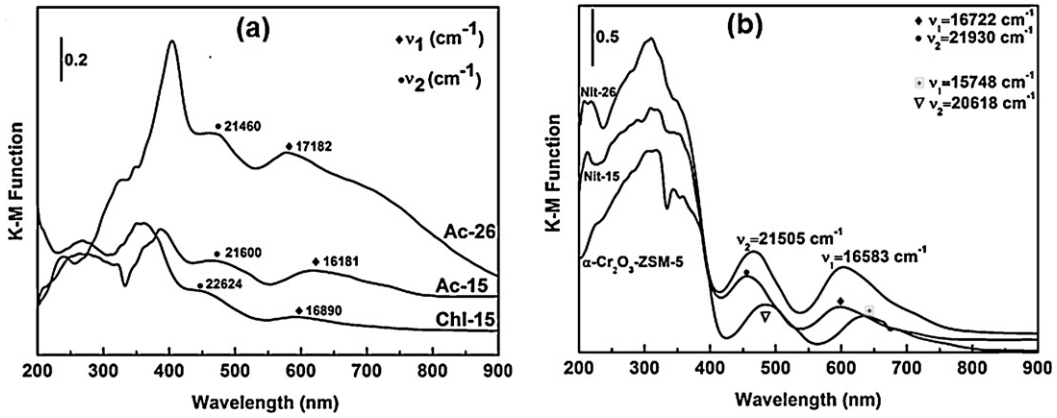

Fig. 5. DRS spectra of (a) Ac-15, Chl-15 and Ac-26 solids, (b) DRS spectra of Nit-15, Nit-26 solids and α-Cr_2O_3-H^+-ZSM-5 (Si/Al = 15) mixture.

υ_1 ($^4A_{2g} \rightarrow {}^4T_{2g}$(F) transition) is equivalent to $10 \times Dq$, and that of υ_2 ($^4A_{2g} \rightarrow {}^4T_{1g}$(F) transition) is given as:

$$\upsilon_2 = 15Dq + \frac{15}{2}B - 6B(1+\mu)^{1/2}$$

where the effective magnetic moment

$$\mu = \left[\frac{10Dq - 9B}{12B}\right]^2$$

and Racah parameter

$$B = \frac{1}{3}\left[\frac{(2\upsilon_1 - \upsilon_2) \times (\upsilon_2 - \upsilon_1)}{9\upsilon_1 - 5\upsilon_2}\right]$$

DRS spectra of the prepared solids are dominated by the support band situated at lower wavelengths [46]. The bands of $O^{2-} \rightarrow Cr^{6+}$ charge transfer (CT) of chromates could be evidenced from the spectra at 267–279 and 346–365 nm [46], while the d–d transition bands of Cr^{3+} ions and/or Cr_2O_3 were detected at 442–465 nm ($^4A_{2g} \rightarrow {}^4T_{1g}$(F) transition) and 582–618 nm ($^4A_{2g} \rightarrow {}^4T_{2g}$(F) transition) [46].

B-value of 457 cm^{-1}, calculated from the DRS spectrum of α-Cr_2O_3-H^+-ZSM-5 mixture (Fig. 5b) and reported in Table 5, does not differ significantly from the value reported in literature [47,48]. According to the orbital theory [45], *B*-value is proportional to the Coulomb integral of e_g and t_{2g} orbitals. Precisely, the increase of *B*-value reflects a decrease in the Cr^{3+}–Cr^{3+} interaction; otherwise, well-crystallized α-Cr_2O_3 oxide exhibits lower *B*-value.

Nit-26 solid exhibited a *B*-value of 458 cm^{-1} which indicates the presence of a crystalline oxide phase at the surface. Nevertheless, the increase in *B*-value suggests that smaller amounts (and/or smaller particles) of α-Cr_2O_3 crystals occupied the surface of Nit-15 sample (with *B*-value of 489 cm^{-1}). These results are in agreement with those of Reinen [47] obtained with a series of $Cr_xAl_{2-x}O_3$ mixed crystals. In fact, the author reported that *B*-values decrease with increasing the concentration of Cr^{3+} ions. Precisely, the increase in *B*-value is due to a decrease in the degree of delocalization of d-electrons onto the ligand as the Cr content decreases. In the case of Ac-15 and Chl-15 solids, with *B*-values of 516 and 548 cm^{-1}, respectively, the interaction in Cr^{3+}-Cr^{3+} is decreased and an amorphous oxide phase takes place. In fact, μ-values of 3.47 and 3.30 BM, respectively for Ac-15 and Chl-15 solids, have been previously reported for amorphous chromia [49–51]. At the contrary, μ-values of 4.50 and 4.40 BM, respectively for α-Cr_2O_3-H^+-ZSM-5 mixture and Nit-15 solid are close to the value obtained with crystalline α-Cr_2O_3 [49,52,53].

Raman spectra of CrO_3-H^+-ZSM-5 and Cr_2O_3-H^+-ZSM-5 mechanical mixtures (Si/Al = 15, 5 wt.% Cr) are presented in Fig. 6, while Raman spectra of the prepared solids are presented in Fig. 7. Parent zeolites do not exhibit any Raman features in the 200–1100 cm^{-1} region and, therefore, all the observed Raman bands are assigned to the vibrations of Cr species. On the other hand, it is important to note that Ac-26 solid does not exhibit any Raman feature because of fluorescence phenomena.

Raman spectrum of CrO_3-H^+-ZSM-5 material exhibited two bands at 374 and 1000 cm^{-1} attributable to the symmetric vibrations of monochromate species and Cr—O vibrations of polychromates, respectively [39,54,55]. On the other hand, Raman spectrum of Cr_2O_3-H^+-ZSM-5 material showed a unique band at 553 cm^{-1} ascribed to Cr—O—Cr vibrations of Cr_2O_3 [39,54].

Based on these results, Raman bands situated at 375 cm^{-1} and 852 cm^{-1} in the spectrum of Chl-15 solid correspond to the vibrations of monochromates [54–56], while the band situated at 548 cm^{-1} is relative to the Cr—O—Cr vibrations of Cr(III) species [39,54]. Similarly, Raman spectra of Ac-15 and Nit-26 solids

Table 5
Position (nm) and assignment of different DRS bands, *B* and μ-parameters values.

Assignment	Ac-15	Nit-15	Chl-15	Ac-26	Nit-26	α-Cr_2O_3-H^+-ZSM-5 (Si/Al = 15) mixture
Support	214	215	164	226	220	–
$O^{2-} \rightarrow Cr^{6+}$ CT of chromates	269360	267365	269356	278 346	279349	––
d–d transitions of Cr^{3+} or Cr_2O_3	463	456	442	466	465	458
	618	598	592	582	603	635
B (cm^{-1})	5163	4894	5483	ND[a]	458–	4574
μ (BM)	.47	.40	.30	–		.50

[a] Not determined due to the unusual aspect of the DRS spectrum.

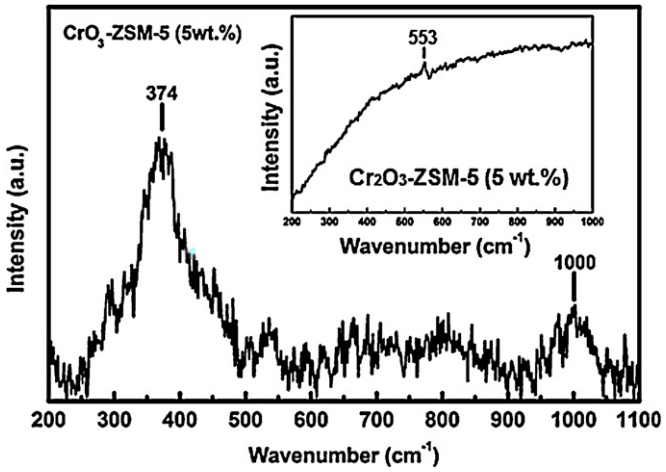

Fig. 6. Raman spectra of CrO_3-H^+-ZSM-5 and Cr_2O_3-H^+-ZSM-5 mechanical mixtures (Si/Al = 15, 5 wt.% Cr).

showed two bands at 295 and 372 cm^{-1}, evidencing the presence of monochromates, and bands at 550 and 555 cm^{-1}, those of octahedral Cr^{3+} species [54]. Nevertheless, Raman spectrum of Nit-15 solid showed bands at 302, 343, 370, 541, 597 and 1007 cm^{-1}. The bands situated at 302 and 370 cm^{-1} would correspond to the vibrations of monochromates, while the ones situated at 343, 541 and 597 cm^{-1} are those of crystalline Cr_2O_3 [12]. The band situated at 1007 cm^{-1} is attributable to the vibrations of polychromate species [54].

Fig. 8a represents XPS spectra of Cr_2O_3-H^+-ZSM-5 mixture (Si/Al = 15, 5 wt.% Cr), Ac-15, Chl-15 and Nit-15 solids, while Fig. 8b represents the deconvolution of XPS spectrum of Cr_2O_3-H^+-ZSM-5 material. Spectral details are presented in Table 6.

In the Fig. 8a, strong Cr 2p signals could be detected for Cr_2O_3-H^+-ZSM-5 material. In contrast, small Cr 2p signals were detected for the rest of samples, evidencing that Cr is incorporated inside the zeolite pores. The deconvolution of XPS spectrum of Cr_2O_3-H^+-ZSM-5 material (Fig. 8b) revealed the presence of two distinct surface species: Cr^{6+} (580 eV) and Cr^{3+} (576.3 eV) [57,58]. The binding energy values, consigned in Table 6, confirm that the surface of different catalysts loaded both Cr^{6+} and Cr^{3+} species. On the other hand, higher amounts of silica occupy the surface since Si/Al ratios determined by XPS exceed their counterparts determined by ICP.

3.5. Redox features

H_2-TPR profiles of the prepared solids are presented in Fig. 9a–e, while TPR profiles obtained with CrO_3 and Cr_2O_3 reference oxides were presented in previous works [39,56,59]. TPR results are compiled in Table 7. It is important to note that amounts of consumed hydrogen were determined by integrating the areas below reduction peaks while maximal temperatures of reduction were determined by deconvolution of TPR profiles into Gaussian bands (see Fig. 9c, for example).

At T_1, the reduction of Cr(VI) species weakly interacted with the zeolite support takes place. However, the formation of Cr(IV) and Cr(V) species like reduction intermediates might occur at the same temperature [60]. The reduction of chromate species anchored to Cr_2O_3 occurs at T_2 [39,56,59], while the reduction of Cr(III) to Cr(II) takes place at T_3 according to Ilieva et al. [61] and based on our experiment performed with pure Cr_2O_3 oxide [39,56,59]. TPR peaks situated at T_4 belong either to the reduction of Cr oxo-cations [39] according to Eq. (3) or to the reduction of chromate species located in the well-accessible channels of ZSM-5 [39].

$$[-O-Cr-O-Cr-O-]^{2+} + 2H_2 \rightarrow 2[Cr(OH)]^{+} + H_2O \quad (3)$$

The peaks situated at T_5 correspond to the reduction of chromates situated in hidden positions inside the zeolite matrix [39].

It is well-known that H/Cr value of 1 corresponds to the reduction of Cr oxide species from +3 to +2 oxidation states, while H/Cr value of 3 corresponds to the reduction of Cr oxide species from +6 to +3 oxidation states. TPR profile of Chl-15 solid (Fig. 9a) showed a unique reduction peak centered at 404 °C and H/Cr molar ratio of ~3 (Table 7) which indicate that chromate species, situated in the more

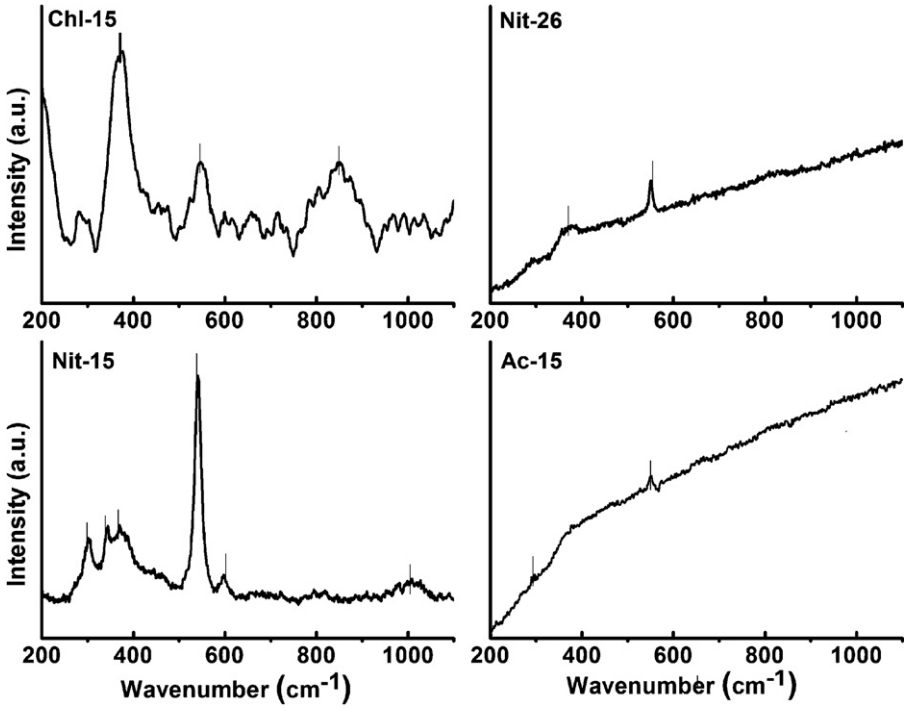

Fig. 7. Raman spectra of the prepared solids.

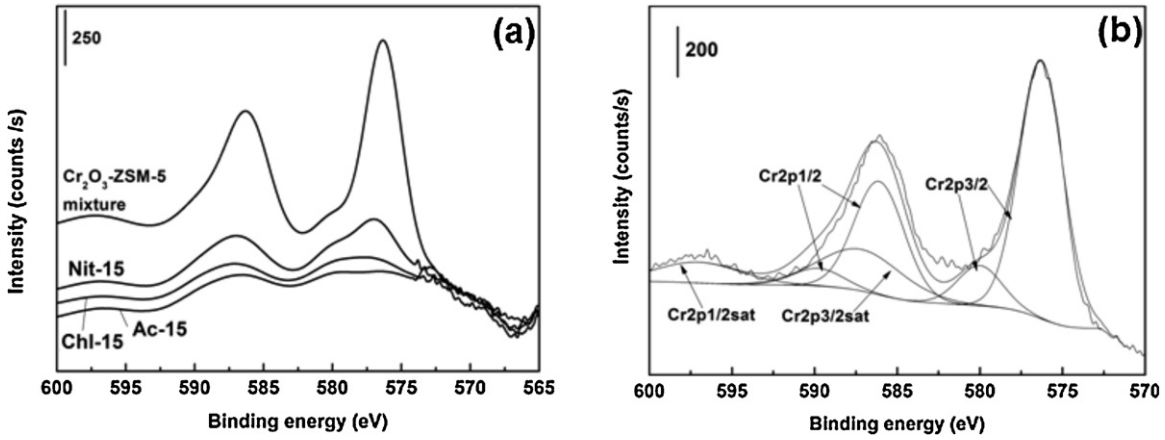

Fig. 8. (a) XPS spectra of Cr_2O_3-H^+-ZSM-5 mixture, Ac-15, Chl-15 and Nit-15 solids, (b) Deconvolution of XPS spectrum of Cr_2O_3-H^+-ZSM-5 mixture.

Table 6
XPS results.

	Ac–15	Chl-15	Nit-15	Cr_2O_3-ZSM-5[a]	Ac-26	Nit-26
Surface atomic ratios						
Cr/Al	0.33	0.38	0.51	0.92	0.70	0.62
Si/Al	20.83	18.51	18.18	9.90	33.33	34.48
Atomic surface concentration (%)						
Cr 2p	0.48	0.62	0.80	2.34	0.64	0.54
Si 2p	30.0	28.9	28.3	25.0	30.1	30.4
Al 2p	1.45	1.57	1.55	2.51	0.89	0.88
Binding energy (eV)						
Cr2p3/2Cr(VI)	580.0	580.0	580.0	580.0	580.0	580.0
Cr2p3/2Cr(III)	576.3	576.9	576.9	576.3	576.7	576.7

[a] Mixture of Cr_2O_3 and H^+-ZSM-5 (Si/Al = 15), Cr amount: 5 wt.%.

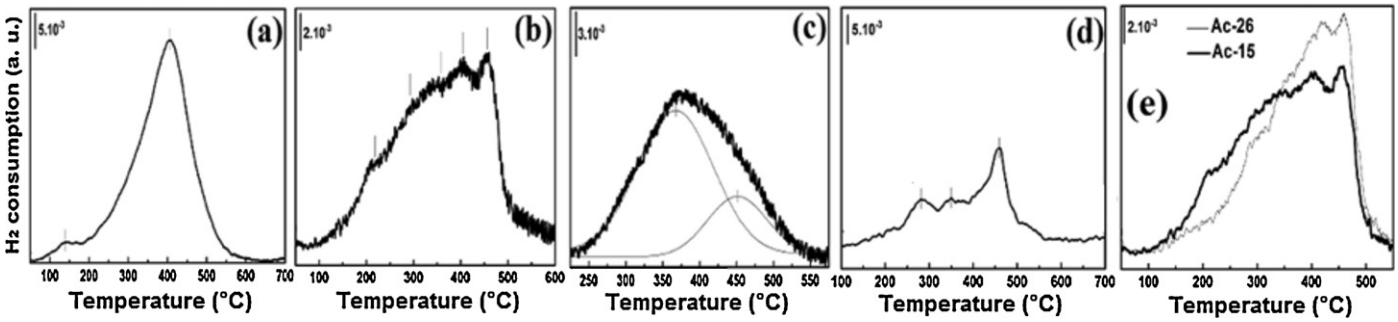

Fig. 9. TPR profiles of (a) Chl-15, (b) Ac-15, (c) Nit-15, (d) Nit-26 solids and (e) Superposition of TPR profiles of Ac-15 and Ac-26 solids.

Table 7
TPR results.

Sample	T_1 (°C)	T_2 (°C)	T_3 (°C)	T_4 (°C)	T_5 (°C)	H/Cr	H_2 amount (mmol H_2/g)	H_2 amount (mmol H_2/g) in regions (a)[a] and (b)[b]
Cr_2O_3 CrO_3 Ac-15	––219	288289292	348–358	––403	– 474/587 454	ND 1.5 0.52	––0 .26	– – 0.12 and 0.14
Ac-26	–	294	361	419	460	0.88	0 .26	0.09 and 0.17
Nit-15	–	–	367	–	451	0.62	0 .27	–
Nit-26	–	281	350	–	460	0.58	0 .12	–
Chl-15	137	–	–	406	–	3.2	0 .49	–

[a] Region (a): 100–360 °C, is the temperature range in which the reduction of surface species occurs.
[b] Region (b): 360–600 °C, is the temperature range in which the reduction of bulk species occurs.

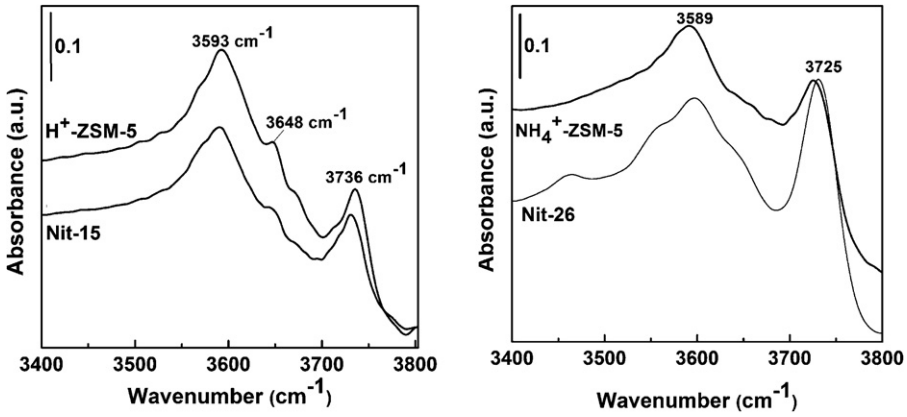

Fig. 10. DRIFT spectra of Nit-15 and Nit-26 solids as well as the corresponding supports.

accessible sites of zeolite, were totally reduced by hydrogen. Nevertheless, over Nit-15 and Nit-26 solids (Fig. 9c and 9d), the reduction of such a species has been inhibited due to the presence of Cr_2O_3 oxide phase. Moreover, Cr species were hardly reduced over Nit-26 solid and required very low amount of hydrogen (0.12 mmol H_2/g) since large particles of crystalline Cr_2O_3 would inhibit the diffusion of hydrogen molecules to the bulk. Accordingly, the easily reduced species over Nit-26 solid are most likely chromates and/or polychromates anchored to the surface of crystalline α-Cr_2O_3. This view could be supported by XPS result obtained with α-Cr_2O_3/zeolite mixture which revealed the presence of surface Cr(VI) species (Fig. 8b).

3.6. NH_3-TPD and DRIFTS studies

The prepared solids as well as the zeolite supports were analyzed by TPD of ammonia in order to determine the global acidity (quantity of ammonia desorbed by 1 g of sample) and the maximal temperatures of desorption. The results are compiled in Table 8. NH_3-TPD profiles of different solids (not presented herein) showed the low temperature desorption peak "l-peak", between 100 and 300 °C, which belongs to the ammonia desorbed from weakly acidic silanol groups [62] and weak Lewis [63] (or Brönsted [64]) acid sites, whereas, the high temperature desorption peak "h-peak", situated between 300 and 600 °C, belongs to the ammonia desorbed from strong acid sites [65]. Amounts of desorbed ammonia will be determined by integrating the areas below desorption peaks in two different temperature regions: regions "a" and "b". Region "a" situated between 100 and 300 °C corresponds to the weakly chimisorbed ammonia, while region "b" corresponds to the strongly chemisorbed ammonia between 300 and 600 °C [65].

The data consigned in Table 8 showed that Ac-15, Chl-15 and H^+-ZSM-5 (Si/Al = 15) samples desorbed similar quantities of ammonia between 300 and 600 °C. At the contrary, throughout the same temperature range, Nit-15 solid desorbed less ammonia quantity than H^+-ZSM-5 does.

In the Table 8, it is also seen that the strength of acid sites, i.e., the amounts of desorbed ammonia as well as the maximal temperatures of desorption, could be correlated. In fact, the more desorbed ammonia, the lower T_h-value is.

A complementary study using DRIFTS might provide additional information about the catalysts acidity. Fig. 10 represents DRIFT spectra of Nit-15 and Nit-26 solids and the corresponding supports.

Spectra of pure zeolites exhibited a band at ~3591 cm^{-1} attributable to Brönsted acid sites [66], a band at 3648 cm^{-1} attributable to Al-OH groups [67] and a band at 3725/3736 cm^{-1} which corresponds to the vibrations of Si-OH groups [68]. The spectra of Nit-15 and Nit-26 solids showed that the intensities of Al-OH and Si-OH bands do not undergo any significant change, suggesting that these groups do not participate significantly in the solid-state reaction. Nevertheless, in the case of Nit-15 solid, the intensity of the band situated at 3591 cm^{-1} decreased, evidencing that Cr ions are exchanged with Brönsted acid sites. The similar trend has been observed with Ac-15, Chl-15 and Ac-26 solids [56,59]. However, Nit-26 solid exhibited a different behavior since the corresponding DRIFT spectrum showed intensive bands due to higher concentrations of hydroxyl groups and, thereby, higher residual acidity.

In summary, using Cr nitrate precursor and NH_4^+-ZSM-5 (Si/Al = 26) like support, the corresponding solid (Nit-26) exhibited a pronounced acidity generated from crystalline oxide species, which behave as Lewis acid sites. However, increasing the Al amount in the case of Nit-15 solid provided more exchange sites for Cr ions than residual acidity. In the case of solids issued from Cr acetate, the less Al containing is the less acidic solid.

Table 8
NH_3-TPD results.

	NH_3 desorbed[a] (mmol NH_3/g)	NH_3 desorbed[b] (mmol NH_3/g)	Global acidity (mmol NH_3/g)	T_l, T_h (°C)
H^+-ZSM-5 (15)	0.65	0.30	0.95	210, 401
Ac-15	0.64	0.29	0.93	207, 395
Chl-15	0.74	0.33	1.07	206, 398
Nit-15	0.49	0.21	0.70	202, 386
NH_4^+-ZSM-5 (26)	0.28	0.55	0.83	204, 410
Ac-26	0.36	0.26	0.62	206, 398
Nit-26	0.41	0.78	1.19	211, 423

[a] Ammonia desorbed between 100 and 300 °C (weakly chemisorbed ammonia).
[b] Ammonia desorbed between 300 and 600 °C (strongly chemisorbed ammonia).

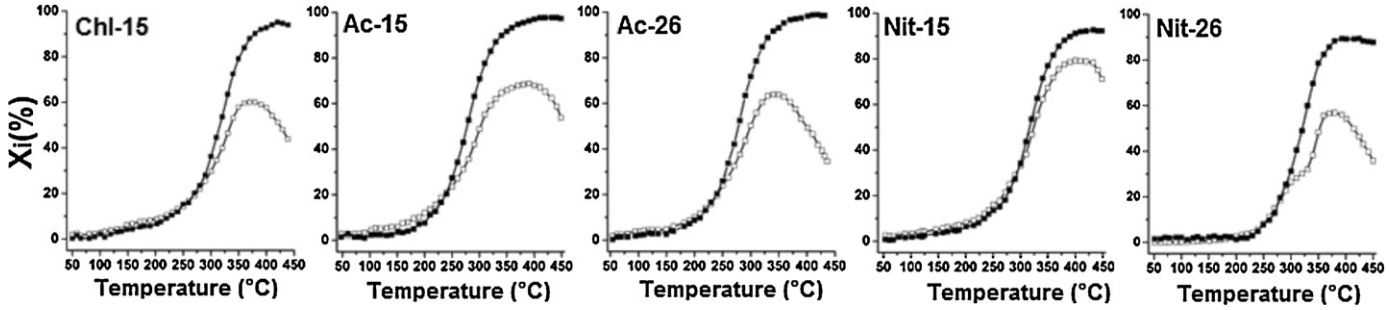

Fig. 11. Conversions of NO (empty square) and NH_3 (full square) as a function of reaction temperature.

Table 9
Catalytic results: N_2O selectivity and NO conversion at particular temperatures.

	T (°C)					S_{N_2O} (%)			X_{NO} (%)		
	T_i	T_{iso}	$T_{N_2O\,max}$	T_{50}	$T_{N_2O\,max}$	T_i	T_{iso}	N_2Omax	T_i	T_{iso}	NO max
Chl-15	200	260	330	335	372	3	14.5	33	9	14.3	60
Nit-15	200	300	310	324	404	3	14.5	24	7.5	33	79
Nit-26	200	280	281	352	376	26	81.5	85	2.1	18	56
Ac-15	200	240	300	302	384	10.5	33	42	11	21	68
Ac-26	200	240	309	302	341	3	21.5	36	10	20	63

Conditions: catalyst weight: 20 mg (activated in situ at 450 °C in air and cooled to room temperature), TPSR from 50 to 450 °C at 7.5 °C/min, space velocity: 332,000 h^{-1}, 2000 ppm NO, 2000 ppm NH_3, 30,000 ppm O_2.

3.7. Catalytic activity

The different catalysts have been tested in SCR of NO in the presence of ammonia. N_2 and H_2O are desirable while N_2O is a side product of SCR process. Fig. 11 represents NO and NH_3 conversions as a function of reaction temperature over Chl-15, Ac-15, Ac-26, Nit-15 and Nit-26 catalysts. The selectivity of such catalysts is the most important of their catalytic properties. However, the comparison of selectivity values obtained at different conversions should be avoided as it might lead to incorrect conclusions. For this reason, the evolution of N_2O selectivity, calculated from molar flows, as a function of reaction temperature is presented in Fig. 12. Furthermore, Table 9 summarizes the catalytic performances of different catalysts at particular temperatures such as $T_i \sim 200$ °C, T_{iso}, T_{50}, and T_{max}. T_{iso} is the temperature in which NO and NH_3 conversion curves deviate noticeably and stop being overlapped, T_{50} stands to the temperature in which 50% of NO conversion was reached while T_{max} are the temperatures of optimal N_2O selectivity and NO conversion. On the other hand, Table 10 recapitulates the selectivity toward N_2 in three different temperature windows: low (50–200 °C), medium (200–250 °C) and high (250–300 °C).

Fig. 11 and Table 9 show that both NO and NH_3 conversion values are slightly similar throughout the temperature range 50–T_{iso}, evidencing that SCR of NO is the predominant reaction. Nevertheless, the unwanted NH_3 oxidation occurs at temperatures above $T_{NO,max}$ since the conversion of NO decreases, while that of NH_3 increases continually and reaches a maximum at higher temperatures.

In the case of Chl-15 catalyst, the SCR process occurs between 50 and 260 °C. Throughout this temperature range, NO conversion reaches 14.3% at $T_{iso} = 260$ °C, while N_2O selectivity increases from 3 for up to 14.5%. At the contrary, SCR of NO occurs between 50 and 300 °C in the case of Nit-15 catalyst. At 260 °C, this catalyst exhibited ~18% of NO conversion and 33% at $T_{iso} = 300$ °C. On the other hand, the data consigned in Table 10 showed that N_2 selectivity varies between 100 and 76% throughout the low, medium and high-temperature windows. These results indicate that both of Nit-15 and Chl-15 catalysts exhibited similar catalytic behaviors in SCR of NO. Nevertheless, Nit-26 solid is very poorly active in SCR. In fact, NO conversion reaches only 18% at $T_{iso} = 280$ °C but the SCR process led to N_2O as main product. The data consigned in Table 10 showed that the selectivity toward N_2 undergoes a significant drop (~80%) throughout the temperature range 50–300 °C. Concerning Cr acetate-issued catalysts, Ac-15 and Ac-26 samples exhibited a temperature window of 50–240 °C for SCR. In this temperature range, similar NO conversions have been reached at T_i, T_{iso} and T_{50} for both catalysts. However, the data consigned in Table 10 showed that Ac-26 catalyst exhibited higher values of N_2 selectivity in the low, medium and high-temperature windows.

At $T = 240$ °C, Chl-15 and Nit-15 catalysts exhibited 85% of selectivity toward N_2, while Nit-26 sample led essentially to the

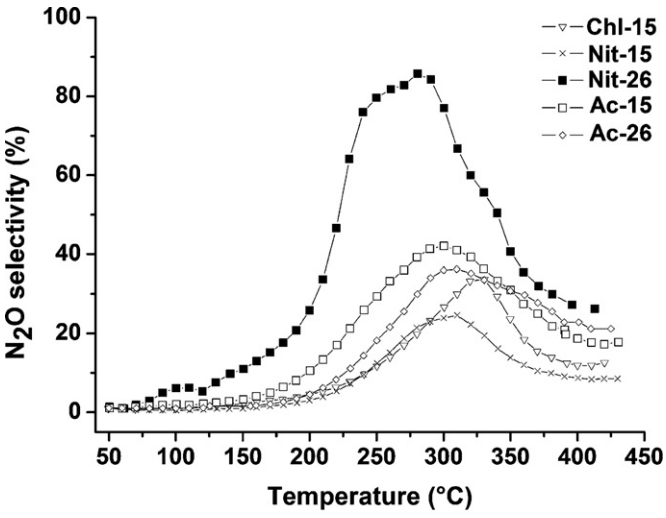

Fig. 12. N_2O selectivity as a function of reaction temperature.

Table 10
N_2 selectivity (%) in low, medium and high-temperature windows.

Temperature window	Chl-15	Nit-15	Nit-26	Ac-15	Ac-26
50–200 °C[a]	100–97	100–97	100–74	100–89.5	100–97
200–250 °C[b]	97–88	97–87	74–20	89.5–70	97–82
250–300 °C[c]	88–73	87–76	20	70–60	82–64

[a] Low-temperature window.
[b] Medium-temperature window.
[c] High-temperature window.

undesired N_2O (N_2 selectivity = 23%). On the other hand, Ac-26 catalyst exhibited narrower SCR temperature window when compared to Chl-15 and Nit-15 catalysts.

Based on the results described above, the catalytic activity of the prepared catalysts increases according to the following sequence: Nit-26 ≪ Ac-15 < Ac-26 < Nit-15&Chl-15. On the other hand, the characterization results showed that Cr speciation varied and depended of two crucial parameters: the nature of Cr precursor and Si/Al molar ratio. In order to facilitate the correlation between the physicochemical and catalytic properties, we need to treat, separately, the influence of the metal precursor nature and Si/Al molar ratio in order to avoid interferences.

When an intimate mixture of Cr precursor (acetate, nitrate or chloride) and ZSM-5 zeolite is heated, the solid-state ion exchange depends of the thermal property of the salt. Whatever the nature of precursor used in this work, the exchange process was accompanied by the migration of Cr ions (present mostly in the form of Cr^{3+}) into zeolite channels according to α-values (Table 3) and XPS results (Fig. 8a). Starting from H^+-ZSM-5 (Si/Al = 15) and $CrCl_3$, the solid-state ion exchange slightly occurs (100% of exchange degree) since the precursor evaporates. However, DRIFTS results [59] showed that the exchange of $CrCl_3$ into H^+-ZSM-5 required Brönsted acid sites, considered as powerful 'traps' for Cr^{3+} ions. On the other hand, the characterization of Chl-15 solid with DRS (Fig. 5a), Raman (Fig. 7) and H_2-TPR (Fig. 9a and Table 7) showed that a part of Cr ions was stabilized inside the zeolite in the form of chromate ions, while TEM micrographs (Fig. 4e) and B/μ-parameter values (Table 5) indicate the presence of some particles of amorphous Cr_2O_3 at the external catalyst surface. In general, chromates (CrO_4^-), strongly anchored to the zeolite and/or established on crystalline chromia (α-Cr_2O_3), as well as polymeric chromates $(Cr_{2+x}O_{7+3x})^{2-}$ are stable species but they exhibited different redox behaviors (Section 3.5).

Using Cr acetate like precursor, the solid-state ion exchange occurred between 250 and 500 °C according to a detailed mechanism previously proposed [39]. On the other hand, TA results (Table 3) showed that Cr acetate salt exhibited a better affinity toward zeolites than $CrCl_3$ does. In fact, Cr(III) ions migrate throughout the channels of ZSM-5 zeolites (Si/Al = 15 and 26) and occupied the exchange sites, essentially Brönsted acid sites [56,59]. However, extending the solid-state reaction for 12 h at 500 °C stabilized Cr ions in the form of monochromate species strongly anchored to the oxygen atoms of the zeolites, while the excess of Cr remains at the outer surface as amorphous Cr_2O_3 particles. In the case of Ac-15 solid, TEM micrographs revealed erratic agglomerates of chromia (Fig. 4a), which suggest a low apparent dispersion, while the micrographs of Ac-26 solid do not reveal developed crystalline phase among zeolite aggregates (Fig. 4b) since wider 10-ring apertures of NH_4^+-ZSM-5 (Si/Al = 26) would facilitate the migration of Cr ions.

In the presence of Cr nitrate, the solid-state exchange occurred successfully as α-values revealed. In fact, the low thermal stability of Cr nitrate salt allows the exchange process at lower temperatures when compared to the rest of precursors (Table 3). After the thermal decomposition of Cr nitrate (below 250 °C), Cr^{3+} ions balancing the negatively charged ZSM-5 frameworks and occupy the exchange sites. In the case of Nit-15 solid, the exchange concerned essentially Brönsted acid sites as DRIFT spectra revealed (Fig. 10). Nevertheless, due to the potential oxidizing power of NO_2, the oxidation of Cr^{3+} into Cr^{6+} as well as the excessive formation of α-Cr_2O_3 followed the thermal decomposition of Cr nitrate. Cr(VI) species are, essentially, mono and polychromates according to Raman results (Fig. 7), while the presence of α-Cr_2O_3 has been evidenced by XRD (Fig. 3). In the case of Nit-26 solid, less-dispersed oxide particles have been detected by TEM (Fig. 4d). Such particles are significantly sized since higher amounts of residual water (Fig. 2) act as binder and enhance the agglomeration of Cr_2O_3 during the thermal treatment of Cr nitrate/NH_4^+-ZSM-5 (Si/Al = 26) mixture.

3.7.1. Catalytic properties of Cr nitrate-issued catalysts

Nit-15 catalyst manifests chromate species strongly anchored to H^+-ZSM-5 (reduced by H_2 at T_5 = 451 °C, Table 5) as well as polymeric chromates (Fig. 7) established on crystalline chromia (α-Cr_2O_3). Such species could be considered as efficient SCR sites throughout the temperature range 50–300 °C since they contain surface oxygen species. It has been reported [69] that SCR of NO over preoxidized Cr_2O_3/Al_2O_3 (9.3%) and pure Cr_2O_3 catalysts takes place mainly on surface oxygens. Similarly, Baiker et col. [70] reported that the higher activity of chromia provided from less-labile (stable) oxygen species. Additionally, the characterization of Nit-15 catalyst revealed the presence of Cr(III) species, sited in the exchange positions (probably in the form of $(CrO)^+$) and/or present as small α-Cr_2O_3 particles. Obviously, the pretreatment of Nit-15 catalyst in air facilitates a coherent coalescence between the small particles of α-Cr_2O_3 to form well-formed crystals of chromia, their external surface being totally accessible to the reactants. Nevertheless, the interaction between chromia particles triggered during the subsequent calcinations (during pretreatment and on-stream) enhances their agglomeration. Thus, large Cr_2O_3 crystal particles outside the zeolite crystals were responsible for the low catalytic activity observed above 300 °C. Concerning Cr oxo-cations, such species could be considered as efficient catalytic sites as reported with Fe/ZSM-5 system [27].

Nit-26 catalyst manifests, as well, chromate species strongly anchored to the support (reduced by H_2 at T_5 = 460 °C, Table 5) and less-dispersed particles of crystalline α-Cr_2O_3. However, the oxidative pretreatment enhances the agglomeration of Cr_2O_3, previously present as massive particles (~50 nm, Fig. 4d). Therefore, crystal particles of chromia with sizes of that order would inhibit the accessibility of chromate species, located in hidden positions in the zeolite framework and considered as efficient catalytic sites, to the reactants. According to TPR study (Section 3.5), the reduction of metallic species over Nit-26 is limited (only 0.12 mmol H_2/g, Table 7) since the oxidative treatment, prior the TPR experiment, enhanced the agglomeration of oxide. Accordingly, the poor catalytic activity of Nit-26 catalyst provided from smaller amounts of surface and bulk chromates (reduced at 281 and 460 °C, respectively) and accessible Cr(III) species (reduced at 350 °C).

Another assumption necessitates to be cited, is that upon Nit-26 catalyst, the acid sites which desorbed ammonia at higher temperature (423 °C, Table 8), are most likely Lewis sites generated from

the Cr exchange (intense DRIFTS bands, Fig. 10). Lewis sites present on crystalline chromia are highly acidic [12] and would catalyze the oxidation of ammonia.

3.7.2. Catalytic properties of Cr acetate-issued catalysts

Komatsu et al. [71] investigated the effect of Si/Al molar ratio on the catalytic properties of Cu/ZSM-5 catalysts in SCR of NO with NH_3. The authors reported that the specific activity increases with the increase of Cu concentration. In fact, the amount of Cu^{2+} which could be introduced in zeolite depends on Al load. Therefore, increasing the Si/Al ratio from 23 to 71 decreased the activity. Nevertheless, in our study, the catalytic behaviors of Ac-15 and Ac-26 catalysts do not follow the trend observed with Cu/ZSM-5 catalysts [71]. In Fig. 9e, TPR profiles of Ac-15 and Ac-26 solids have been superposed in order to demonstrate the difference in their redox properties. On the other hand, the amounts of consumed hydrogen in two different temperature regions have been summarized in Table 7 (last column). In the case of Ac-15 solid, the reduction of surface (anchored to the surface of Cr_2O_3) and bulk (sited in well-accessible and hidden positions of zeolite) chromate species required 0.12 and 0.14 mmol H_2/g, respectively. However, in the case of Ac-26 solid, the reduction of such species required 0.09 and 0.17 mmol H_2/g, respectively. These results would provide information about the oxide phase developed at the catalysts surfaces. In fact, the surface of Ac-15 solid exhibits a well-developed oxide phase which inhibited the reduction of bulk chromates at $T > 360\,^{\circ}C$. At the contrary, at $T < 360\,^{\circ}C$, the reduction of surface chromates required less hydrogen amount in the case of Ac-26 solid. TEM micrographs (Fig. 4a and b) agreed the TPR results since Ac-15 solid manifested, initially, erratic agglomerates of amorphous chromia while neither crystalline phase nor agglomerates were detected at the surface of Ac-26 solid. Consequently, the pronounced formation of N_2O over Ac-15 catalyst provided essentially from oxide agglomerates, which either inhibit the diffusion of reactant to the hidden chromates or enhance the secondary reaction.

3.7.3. Catalytic property of Cr chloride-issued catalyst

Using Cr chloride like precursor, the corresponding catalyst exhibited higher activity and selectivity toward N_2. The characterization results revealed the presence of chromates, sited in accessible framework positions, as well as clusters of Cr_2O_3 oxide which could be considered as active sites.

4. Conclusion

Cr exchanged ZSM-5 catalysts prepared by solid-state ion exchange from different chromium salts (acetate, chloride and nitrate) were tested in SCR of NO in the presence of ammonia. Characterization results revealed that Cr speciation depended of two crucial preparation parameters; the nature of precursor and Si/Al molar ratio. Since $CrCl_3$ precursor evaporates in the solid-state exchange condition, Cr_2O_3 formation occurs to a low extent and the predominant species are chromates sited in accessible positions of H^+-ZSM-5 (Si/Al = 15) zeolite framework. Starting form Cr nitrate like precursor and NH_4^+-ZSM-5 support (Si/Al = 26), α-Cr_2O_3 particles of significant size occupied the surface. However, using the same precursor and H^+-ZSM-5 (Si/Al = 15) like support, mono (and poly) chromate species, Cr oxo-cations and well-dispersed crystals of α-Cr_2O_3 coexist. Moreover, starting from Cr acetate precursor, the morphology of oxide species at the catalysts surface depended of the nature of zeolite support. The catalytic activity of the prepared catalysts increases according to the following sequence: Nit-26 ≪ Ac-15 < Ac-26 < Nit-15&Chl-15. The catalysts issued from Cr chloride and Cr nitrate like precursors and H^+-ZSM-5 (Si/Al = 15) like support exhibited higher catalytic activity. However, the catalysts issued from Cr acetate precursor were active in SCR but agglomerates of Cr_2O_3 must be avoided with H^+-ZSM-5 (Si/Al = 15) like support, mainly with oxidative pretreatment. On the other hand, using Cr nitrate and NH_4^+-ZSM-5 (Si/Al = 26), the corresponding catalyst is poorly active since massive particles of Cr oxide encourage the oxidation of ammonia and inhibit the accessibility of hidden chromate species to the reactants. It seems that Cr oxo-cations, oxide clusters as well as surface and bulk chromate species are active in SCR of NO while massive particles of Cr oxide (amorphous or crystalline chromia) inhibit the accessibility of active sites to the reactants and enhance the secondary reaction. Insignificant production of N_2O has been observed at low (50–200 °C), medium (200–250 °C) and high (250–300 °C) temperature windows with most of the prepared catalysts. Consequently, the finding of this work will be used to explain the catalytic behavior of Cr exchanged zeolite catalysts in SCR of NO with NH_3, being abandoned, and further investigations could render such catalysts more attractive.

References

[1] World Databank, World Development Indicators (WDI) and Global Development Finance (GDF).
[2] G. Busca, L. Lietti, G. Ramis, F. Berti, Applied Catalysis B: Environmental 18 (1998) 1–35.
[3] A. Bahamonde, A. Beretta, P. Avila, E. Troconi, Industrial and Engineering Chemistry Research 35 (1996) 2516–2521.
[4] A. Beretta, C. Orsenigo, N. Ferlazzo, E. Troconi, P. Forzattti, Industrial and Engineering Chemistry Research 37 (1998) 2623–2633.
[5] T.S. Park, S.K. Jeong, S.H. Hong, S.Ch. Hong, Industrial and Engineering Chemistry Research 40 (2001) 4491–4495.
[6] J. Muniz, G. Marban, A.B. Fuertes, Applied Catalysis B: Environmental 23 (1999) 25–35.
[7] E. Zhu, Z. Liu, S. Liu, H. Niu, T. Hu, T. Liu, Y. Xie, Applied Catalysis B: Environmental 26 (2000) 25–35.
[8] L. Singoredjo, R. Korver, F. Kapteijn, J. Moulijn, Applied Catalysis B: Environmental 1 (1992) 297–316.
[9] B. Huang, R. Huang, D. Jin, D. Ye, Catalysis Today 126 (2007) 279–283.
[10] R.Q. Long, R.T. Yang, R. Chang, Catalysis Communications (2002) 452–453.
[11] J. Li, H. Chang, L. Ma, J. Hao, R.T. Yang, Catalysis Today 175 (2011) 147–156.
[12] H.E. Curry-Hyde, H. Musch, A. Baiker, M. Schraml-Marth, A. Wokaun, Journal of Catalysis 133 (1992) 397–414.
[13] K. Köhler, C.W. Schläpfer, A. von Zelewsky, J. Nickl, J. Engweiler, A. Baiker, Journal of Catalysis 143 (1993) 201–214.
[14] Ch. Fountzoula, H.K. Matralis, Ch. Papadopoulou, G.A. Voyiatzis, Ch. Kordulis, Journal of Catalysis 172 (1997) 391–405.
[15] J. Słoczyński, J. Janas, T. Machej, J. Rynkowski, J. Stoch, Applied Catalysis B: Environmental 24 (2000) 45–60.
[16] F. Ayari, M. Mhamdi, G. Delahay, A. Ghorbel, Journal of Porous Materials 17 (2010) 265–274.
[17] H. Schneider, S. Tschudin, M. Schneider, A. Wokaun, A. Baiker, Journal of Catalysis 147 (1994) 5–14.
[18] J. Engweiler, J. Nickl, A. Baiker, K. Khöler, C.W. Schläpfer, A. von Zelewsky, Journal of Catalysis 145 (1994) 141–150.
[19] U. Scharf, H. Schneider, A. Baiker, A. Wokaun, Journal of Catalysis 145 (1994) 464–478.
[20] A.Z. Ma, W. Grunert, Catalysis Communications (1999) 71–72.
[21] M. Richter, A. Trunschke, U. Bentrup, K.W. Brzezinka, E. Schreier, M. Schneider, M.M. Pohl, R. Fricke, Journal of Catalysis 206 (2002) 98–113.
[22] J.H. Baik, S.D. Yim, I.S. Nam, Y.S. Mok, J.H. Lee, B.K. Cho, S.H. Oh, Topics in Catalysis 30/31 (2004) 37–41.
[23] G. Carja, Y. Kameshima, K. Okada, C.D. Madhusoodana, Applied Catalysis B: Environmental 73 (2007) 60–64.
[24] E.Y. Choi, I.S. Nam, Y.G. Kim, Journal of Catalysis 161 (1996) 597–604.
[25] K. Rahkamaa-Tolonen, T. Maunula, M. Lomma, M. Huuhtanen, R.L. Keiski, Catalysis Today 100 (2005) 217–222.
[26] T. Seiyama, T. Arakawa, T. Matsuda, Y. Takita, N. Yamazoe, Journal of Catalysis 48 (1977) 1–7.
[27] G. Delahay, D. Valade, A.G. Vargas, B. Coq, Applied Catalysis B: Environmental 55 (2005) 149–155.
[28] G.S. Qi, R.T. Yang, Applied Catalysis B: Environmental 60 (2005) 13–22.
[29] R.Q. Long, R.T. Yang, Catalysis Letters 74 (2001) 201–205.
[30] H.Y. Chen, W.M.H. Sachtler, Catalysis Letters 50 (1998) 125–130.
[31] A.V. Salker, W. Weisweiler, Applied Catalysis A: General 203 (2000) 221–229.
[32] Ch. Baerlocher, W.M. Meier, D.H. Olson (Eds.), Atlas of Zeolite Framework Types, 5th revised ed., Elsevier, Amsterdam, 2001.
[33] N.E. Fouad, H. Knözinguer, M.I. Zaki, S.A.A. Mansour, Zeitschrift fur Physikalische Chemie 171 (1991) 75–96.
[34] A. Małecki, B. Małecka, R. Gajerski, S. Labu, Journal of Thermal Analysis and Calorimetry 72 (2003) 135–144.

[35] L.N. Zelenina, Z.I. Titov, T.P. Chusova, Russian Chemical Bulletin 53 (8) (2004) 1621–1624.
[36] V. Plies, Zeitschrift fur Anorganische und Allgemeine Chemie 556 (1988) 120–128.
[37] K.C. Sole, M.B. Moolman, M.E. Brown, Journal of the Chemical Society, Faraday Transactions 86 (3) (1990) 525–530.
[38] L. Li, Z.F. Yan, G.Q. Lu, Z.H. Zhu, Journal of Physical Chemistry B 110 (2006) 178–183.
[39] F. Ayari, M. Mhamdi, T. Hammedi, J. Álvarez-Rodríguez, A.R. Guerrero-Ruiz, G. Delahay, A. Ghorbel, Applied Catalysis A: General 439/440 (2012) 88–100.
[40] V.P. Mavrodinova, Microporous and Mesoporous Materials 24 (1998) 9–18.
[41] A. Gervasini, Applied Catalysis A: General 180 (1999) 71–82.
[42] M.M.J. Treacy, J.B. Higgins, Collection of Simulated XRD Powder Patterns for Zeolites, 4th ed., Elsevier, Amsterdam, 2001.
[43] A.R. West, Solid State Chemistry and its Applications, Wiley, New York, 1989.
[44] C. Covarrubias, R. García, R. Arriagada, J. Yánez, M.T. Garland, Microporous and Mesoporous Materials 88 (2006) 220–231.
[45] R.M. Abu-Eid, R.G. Burns, American Mineralogist 61 (1976) 391–397.
[46] B.M. Weckhuysen, H.J. Spooren, R.A. Schoonheydt, Zeolites 14 (1994) 450–457.
[47] D. Reinen, in: Structure and Bonding, vol. 6, Springer-Verlag, Berlin, 1969, pp. 30–51.
[48] F. Cavani, M. Koutyrev, F. Trifirò, A. Bartolini, D. Ghisletti, R. Iezzi, A. Santucci, G. Del Piero, Journal of Catalysis 158 (1996) 236–250.
[49] A. Ellison, J.O.V. Oubridge, K.S.W. Sing, Transactions of the Faraday Society 66 (1970) 1004–1014.
[50] E.J. Fiebele, N.C. Koon, L.K. Wilson, D.L. Kinser, Journal of the American Ceramic Society 57 (1974) 237–241.
[51] I. Ardelean, S. Filip, Journal of Optoelectronics and Advanced Materials 7 (2005) 745–752.
[52] F.S. Stone, J.C. Vickerman, Transactions of the Faraday Society 67 (1971) 316–328.
[53] I. Pop, M. Andercut, I. Burda, C. Oprea, C. Andercut, Journal of Materials Science Letters 16 (1997) 2052–2054.
[54] B.M. Weckhuysen, I.E. Wachs, R. Schoonheydt, Chemical Reviews 96 (1996) 3327–3349.
[55] M.A. Vuurman, I.E. Wachs, Journal of Physical Chemistry 96 (1992) 5008–5016.
[56] F. Ayari, M. Mhamdi, J. Álvarez-Rodríguez, A.R. Guerrero-Ruiz, G. Delahay, A. Ghorbel, Applied Catalysis A: General 415–416 (2012) 132–140.
[57] F. Simard, U.A. Sedran, J. Sepũ1veda, N.S. Fîgoli, H.I. de Lasa, Applied Catalysis A: General 125 (1995) 81–98.
[58] NIST X-Ray Photoelectron Spectroscopy Database, NIST Standard Reference Database 20, Version 3.5.
[59] F. Ayari, M. Mhamdi, D.P. Debecker, E.M. Gaigneaux, J. Álvarez-Rodríguez, A.R. Guerrero-Ruiz, G. Delahay, A. Ghorbel, Journal of Molecular Catalysis A: Chemical 339 (2011) 8–16.
[60] L.R.R. de Araujo, M. Schmal, Applied Catalysis A: General 235 (2002) 139–147.
[61] L.I. Ilieva, D.H. Andreeva, Thermochimica Acta 265 (1995) 223–231.
[62] N.-Y. Topsoe, K. Pedersen, E.G. Derouane, Journal of Catalysis 70 (1981) 41–52.
[63] H.G Karge, in: G. Öhlmann, H. Pfeifer, R. Fricke (Eds.), Catalysis and Adsorption by Zeolites, Stud. Surf. Sci. Catal., vol. 65, Elsevier, Amsterdam, 1991, p. 133.
[64] C.V. Hidalgo, H. Itoh, T. Hattori, M. Niwa, Y. Murakami, Journal of Catalysis 85 (1984) 362–369.
[65] F. Lónyi, J. Valyon, Microporous and Mesoporous Materials 47 (2001) 293–301.
[66] A.W. Chesr, R.M. Dessarn, L.B. Alemani, G.J. Woolevy, Zeolites 6 (1986) 14–16.
[67] E. Gallei, D. Eisenbach, Journal of Catalysis 37 (1975) 474–485.
[68] A. Jentys, G. Rumplmayr, J.A. Lercher, Applied Catalysis 53 (1989) 299–312.
[69] H. Niiyama, K. Murata, E. Echigoya, Journal of Catalysis 48 (1977) 201–208.
[70] H.E. Curry-Hyde, H. Musch, A. Baiker, Applied Catalysis 65 (1990) 211–223.
[71] T. Komatsu, M. Nunokawa, I.S. Moon, T. Takahara, S. Namba, T. Yashima, Journal of Catalysis 148 (1994) 427–437.